Supplementary material for LHCb-PAPER-2017-045

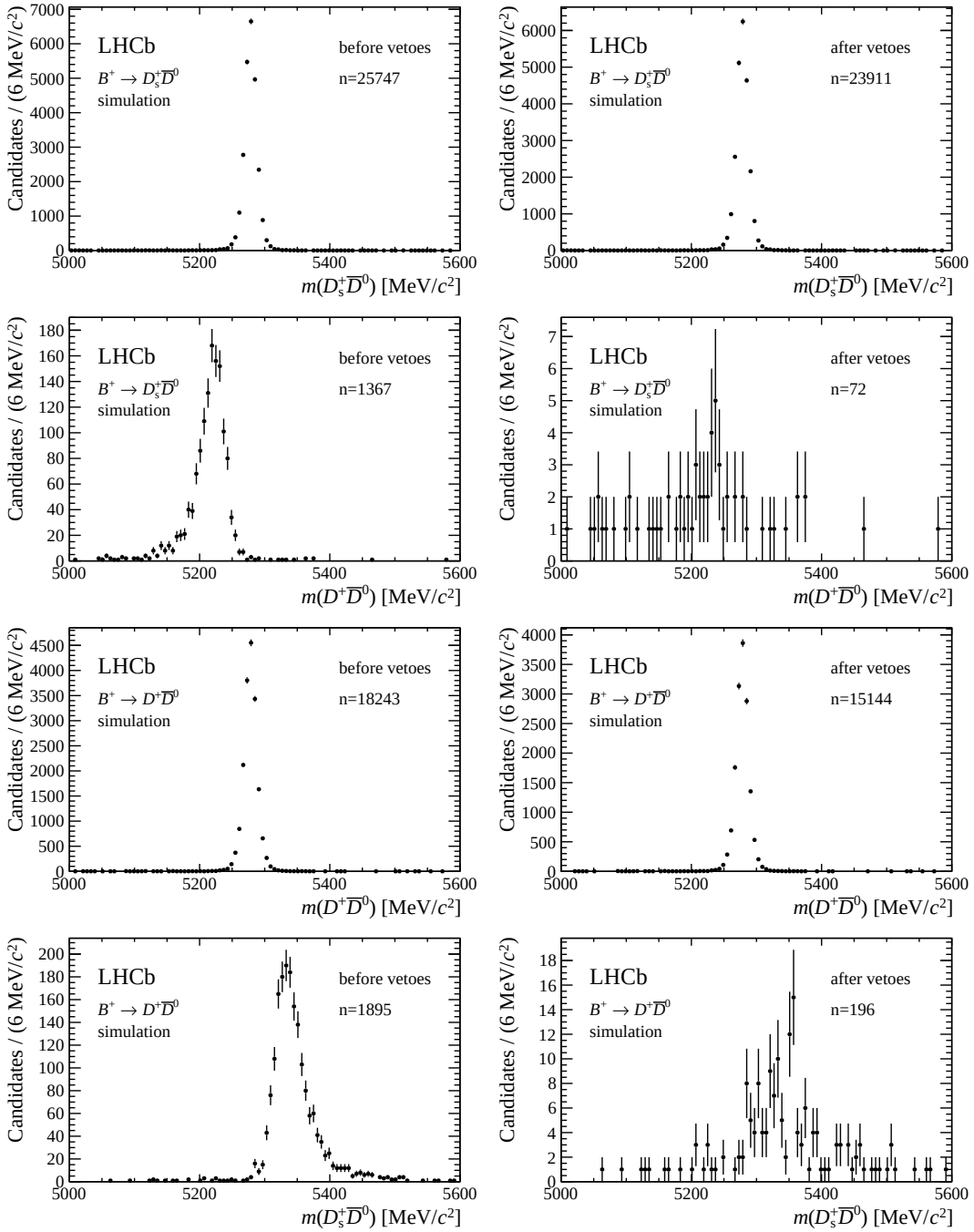

Figure 1: Distributions of the invariant mass of $B^+ \to D^+_{(s)}\overline{D}^0$ candidates with $D^0 \to K^-\pi^+$ decays from simulated $B^+ \to D^+_{(s)}\overline{D}^0$ events, with the number of entries, n, indicated (left) before and (right) after the cross-feed vetoes. Top-row plots are for simulated $D_s^+\overline{D}^0$ events, reconstructed as $D_s^+\overline{D}^0$. Second-row plots are for simulated $D_s^+\overline{D}^0$ events, reconstructed as $D^+\overline{D}^0$. Third-row plots are for simulated $D^+\overline{D}^0$ events, reconstructed as $D^+\overline{D}^0$. Bottom-row plots are for simulated $D^+\overline{D}^0$ events, reconstructed as $D_s^+\overline{D}^0$.

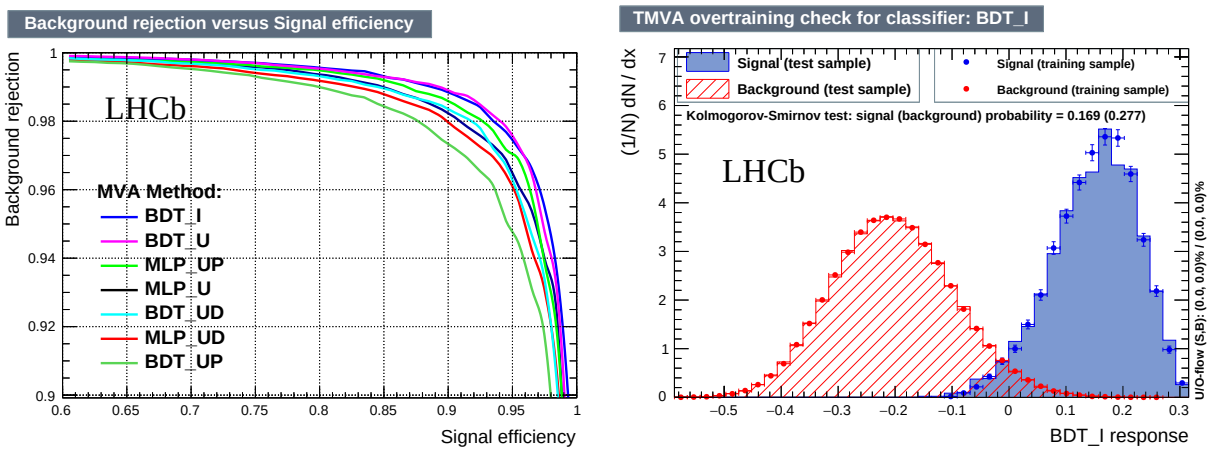

Figure 2: (left) Comparison of the performance of several classifiers, evaluated for the selection of $B_c^+ \to D_s^+ \overline{D}^0$ decays. The two classifiers considered are boosted decision tree (BDT) and multilayer perceptron (MLP). Several transformations of the input variables are considered: I for identity (no transformation), U for uniform (transform such that the sum of signal and background distribution is uniform), P for principal component decomposition, and D for decorrelation. (right) Output distributions of the BDT for $B_c^+ \to D_s^+ \overline{D}^0$ decays, followed by $D^0 \to K^-\pi^+$. Signal and background distributions are compared and the testing and training samples are overlaid.

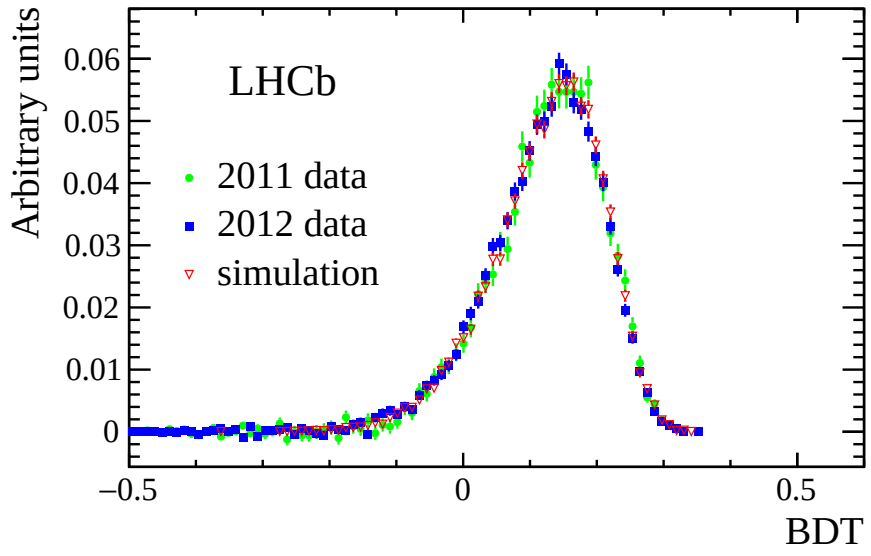

Figure 3: Comparison of the BDT response between data and simulation for $B^+ \to D_s^+ \overline{D}^0$ decays. For the data, the background has been subtracted using sWeights, where the weight was determined from the reconstructed invariant mass of the B^+ candidate.

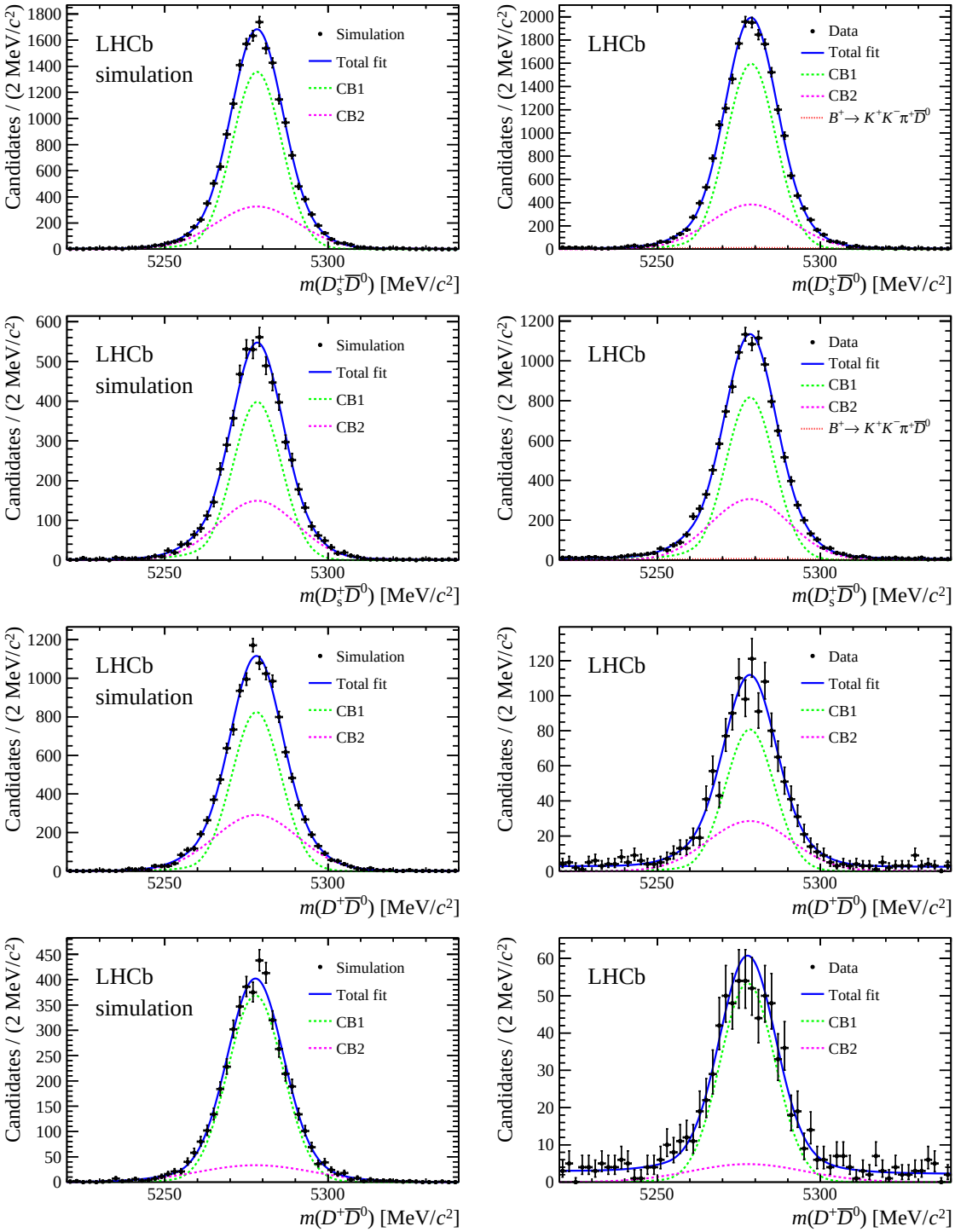

Figure 4: Reconstructed invariant-mass distributions of $B^+ \to D^+_{(s)}\overline{D}^0$ candidates; left are from simulation and right are from data. Top row are $D_s^+\overline{D}^0$ with $D^0 \to K^-\pi^+$ final states, second row are $D_s^+\overline{D}^0$ with $D^0 \to K^-\pi^+\pi^-\pi^+$, third row are $D^+\overline{D}^0$ with $D^0 \to K^-\pi^+$ and on the bottom row are $D^+\overline{D}^0$ with $D^0 \to K^-\pi^+\pi^-\pi^+$. Overlaid are fits to a double Crystal Ball function plus background components. For the simulation, the shape parameters are floating, while for the data all shape parameters have been fixed to the values obtained from the fit to the simulated events.

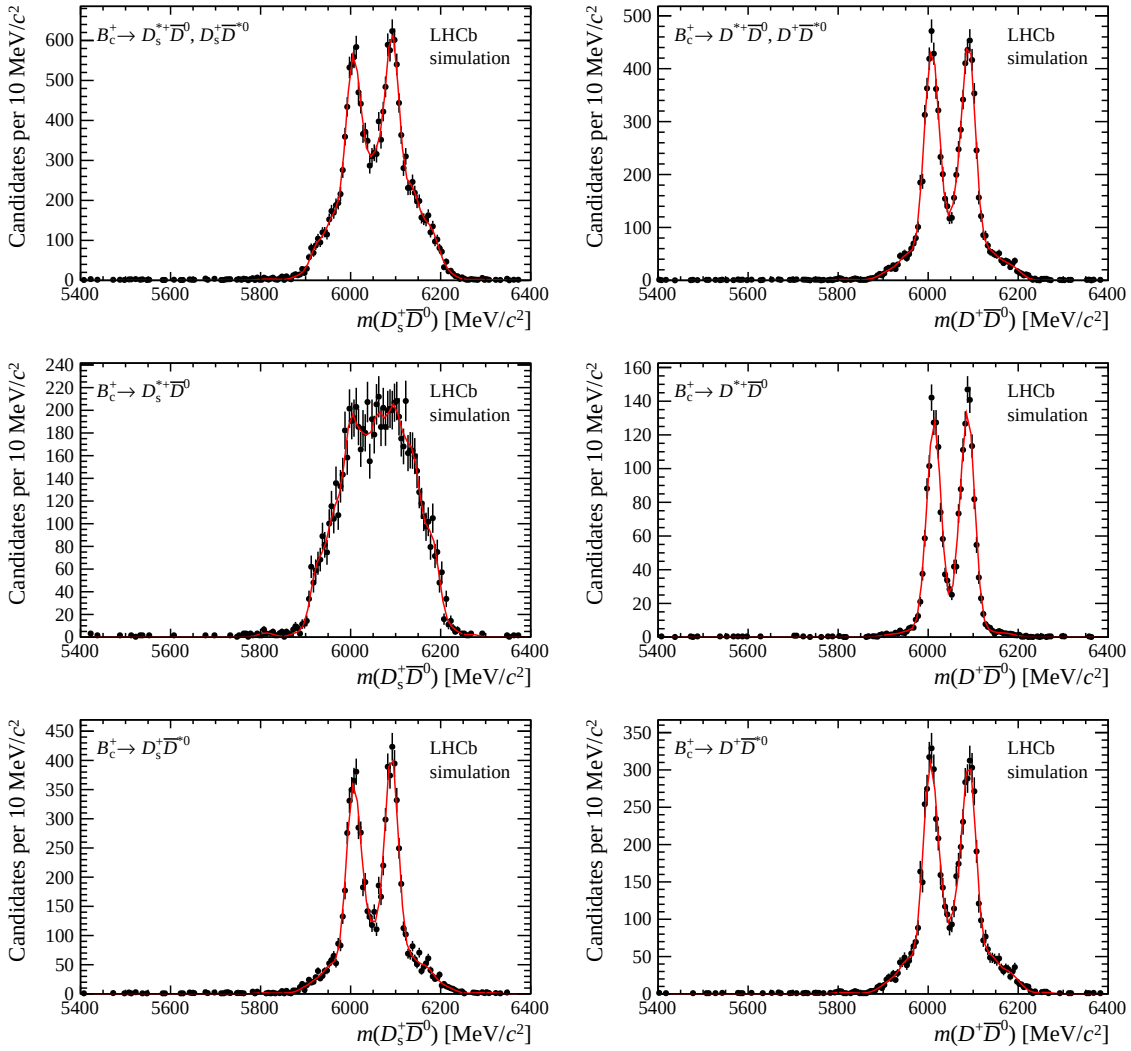

Figure 5: Reconstructed invariant-mass distributions of $B_c^+ \to D_{(s)}^{*+}\overline{D}^0, D_{(s)}^+\overline{D}^{*0}$, $D^0 \to K^-\pi^+$ candidates from simulation. The top-row figures show the weighted sum of the two components (shown in the middle and bottom row). The middle- and bottom-row figures show the individual components, used for the systematic studies. Fits to a sum of Gaussian functions are overlaid.

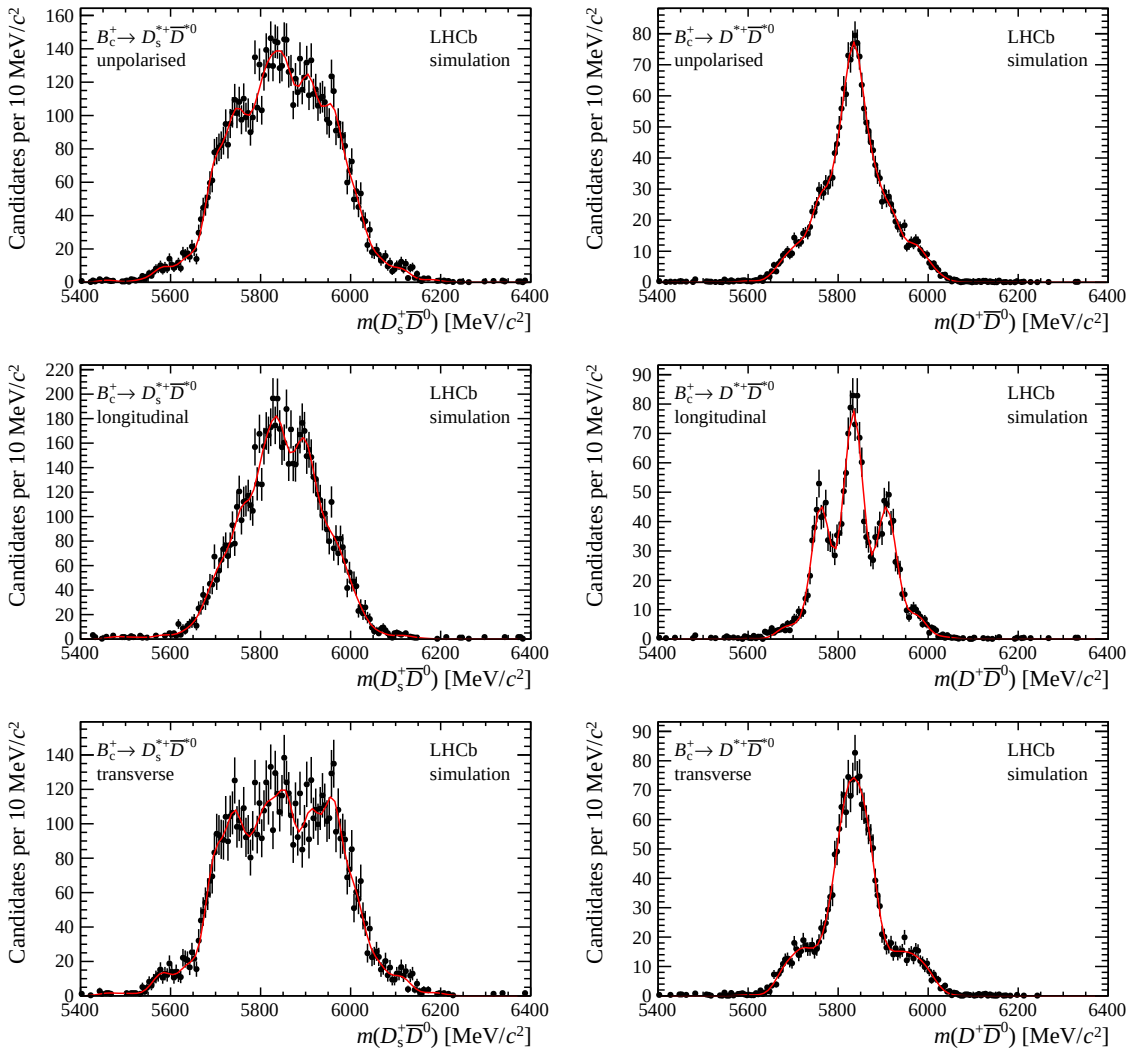

Figure 6: Reconstructed invariant-mass distributions of $B_c^+ \to D_{(s)}^{*+}\overline{D}^{*0}$, $D^0 \to K^-\pi^+$ candidates from simulation. The top-row figures show the weighted sum of the two components (shown in the middle and bottom row). The middle- and bottom-row figures show the individual components, used for the systematic studies. Fits to a sum of Gaussian functions are overlaid.

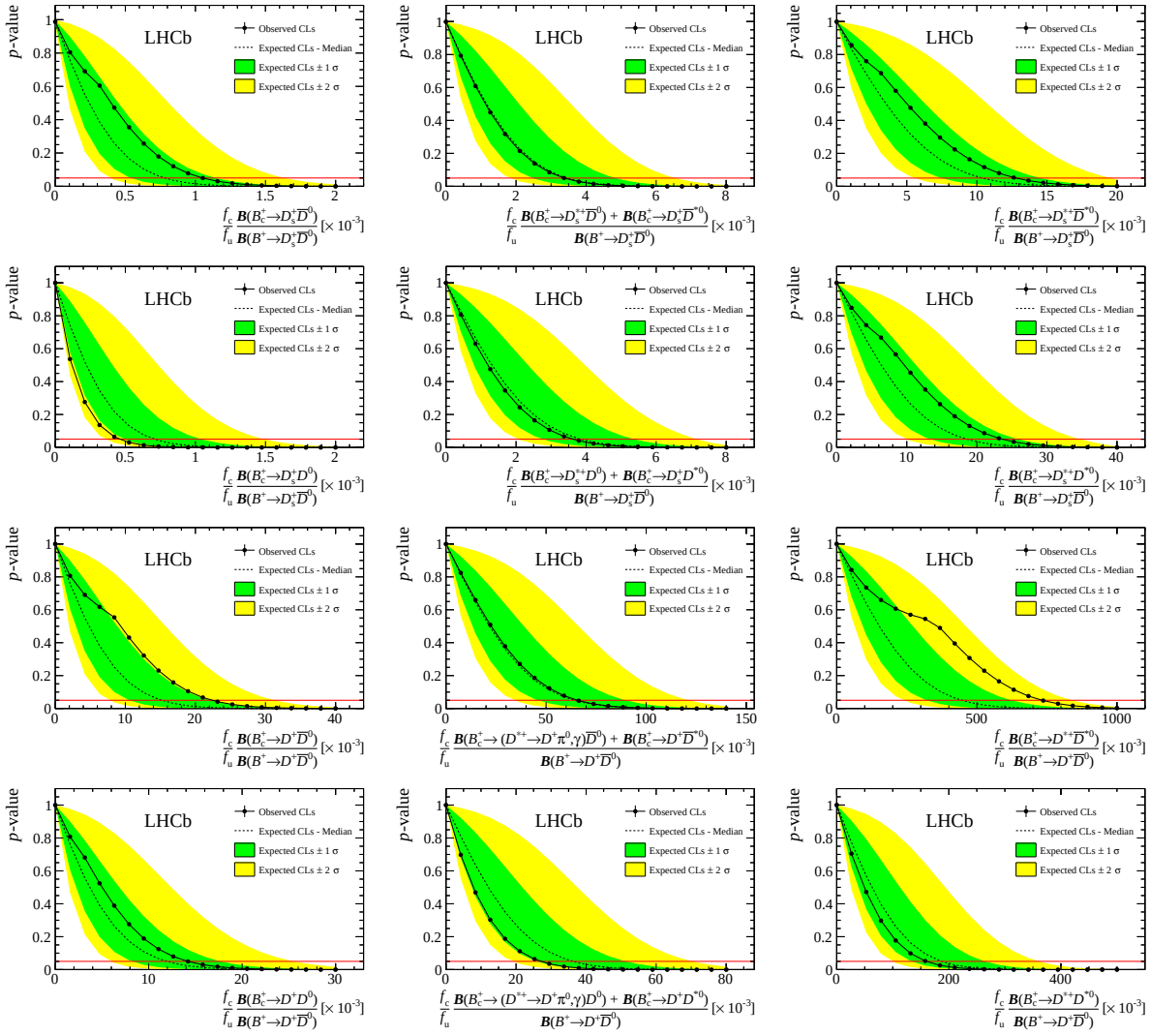

Figure 7: CL$_s$ p-value distributions for the measured values of $\frac{f_c}{f_u}\frac{\mathcal{B}(B_c^+\to D_{(s)}^{(*)+}D^{(*)})}{\mathcal{B}(B^+\to D_{(s)}^+\overline{D}^0)}$. Top plots are for $B_c^+\to D_s^+\overline{D}^0$ final states, the second row for $B_c^+\to D_s^+D^0$ final states, the third row for $B_c^+\to D^+\overline{D}^0$ final states, and the bottom row for $B_c^+\to D^+D^0$ final states. Left plots are for $B_c^+\to D_{(s)}^+D$ decays, middle plots are for $B_c^+\to D_{(s)}^{*+}D, D_{(s)}^+D^*$, and right plots for $B_c^+\to D_{(s)}^{*+}D^*$. The intersections of the horizontal red lines with the black solid curves correspond to the limits at 95% confidence level.